A Mathematical Model for the Distribution of Fluorodeoxyglucose in Humans

Marguerite T. Hays and George M. Segall

Nuclear Medicine Service, Veterans Affairs Palo Alto Health Care System, Palo Alto, and Department of Radiology, Stanford University, Stanford, California

The goals of this study were to define the total body distribution kinetics of ^{18}F-fluorodeoxyglucose (FDG), to contribute to its radiation dosimetry and to define a suitable proxy for arterial cannulation in human FDG studies. **Methods:** Time-activity FDG heart, lung, liver and blood data from paired fasting and glucose-loaded sessions in five adult human volunteers, together with published brain parameters, were incorporated into a multicompartmental model for whole-body FDG kinetics. Tau values were calculated from this model. We also compared the usefulness of activity in the left ventricle (LV), right ventricle (RV), left lung and right lung as proxy for arterial blood FDG sampling. **Results:** No systematic difference was found in model parameters between the fasting and glucose-fed sessions, even for the parameter for transfer of FDG into the myocardium. Myocardial PET data fitted well to a model in which there is very rapid exchange indistinguishable from blood kinetics and transfer into an intracellular "sink." The lung data fitted to a simple sink representing the lung cells. The liver data required an additional intermediate exchange compartment between the plasma and a hepatic sink. In terms of total body distribution kinetics, unmeasured organs and tissues (probably the skeletal muscle and gut) become increasingly important with time and account for a mean of 76% of the decay-corrected FDG activity at infinity. Right lung activity, corrected to venous blood, represents the whole arterial blood curve better than the LV or RV. The tau values for radiation dosimetry of FDG in the heart, lungs, liver and bladder calculated from our model do not differ significantly from published results using other methods. Bladder tau decreased with voiding frequency and was markedly decreased with early voiding. **Conclusion:** Glucose loading state is not a good predictor of myocardial FDG uptake. The majority of FDG distribution at 90 min is in tissues other than the blood, brain, heart and liver. Bladder radiation will be much reduced if the patient voids early after FDG administration. Summed large volume right lung activity, normalized to venous blood activity, is a good proxy for arterial blood FDG sampling. The model presented may be expanded to include other FDG kinetics as studies become available.

Key Words: compartmental model; fluorodeoxyglucose; radiation dosimetry

J Nucl Med 1998; 40:1358–1366

Received Aug. 14, 1998; revision accepted Jan. 20, 1999.

For correspondence or reprints contact: Marguerite T. Hays, MD (115), VA Palo Alto Health Care System, 3801 Miranda Ave., Palo Alto, CA 94304.

With the increasing use of ^{18}F-fluorodeoxyglucose (FDG) in clinical nuclear medicine, it is important to delineate its normal distribution in humans. One of the most urgent needs for understanding FDG distribution kinetics is to establish its radiation dosimetry. Several studies in the literature have provided estimates of radiation dose to the brain, bladder and other organs (*1,2*), but there has not previously been an attempt to synthesize these observations into a unified kinetic model.

The Medical Internal Radiation Dose (MIRD) Committee of the Society of Nuclear Medicine has undertaken the preparation of a dose estimate report for FDG. After reviewing the available published and unpublished kinetic data, the Committee identified a need for more data about FDG kinetics in the organs other than the brain. It was to meet this need that we undertook this study, in which we have measured FDG kinetics in the plasma, erythrocytes, heart, lungs and liver directly. To complete the picture of the most important organs of FDG distribution, we have also incorporated into our model published parameters describing brain FDG kinetics (*3*).

MATERIALS AND METHODS

Participants

Five adult volunteers (four men, one woman) were the participants in this study. Each participant was involved in two complete study sessions. Data from two other participants (whose blood data are incomplete) will be incorporated into the MIRD Dose Estimate Report but were not included in this study. Each volunteer had normal myocardial function as defined by a negative stress cardiac study performed for clinical indications in the Nuclear Medicine Service, Veterans Affairs Palo Alto Health Care System (Palo Alto, CA). Participants were informed fully about the purposes and procedures of the study and gave written consent. This study was approved and monitored by the Stanford University Institutional Review Board.

Study Procedure

Two study sessions for each participant, approximately 1 wk apart, were identical, except for the administration of glucose. Participants arrived at the laboratory fasting, but in one of the two sessions (the first for three participants and the second for two participants), they received 90 g glucose orally 1 h before FDG injection, and blood sugar was measured just before tracer administration. After the investigator discussed the study with the partici-

pants, a physician from the anesthesiology service placed an arterial line for blood sampling in a radial artery.

Imaging was performed in a dedicated bismuth germanate crystal PET scanner (ECAT EXACT; CTI, Knoxville, TN) with a 16.2-cm field of view, 47 transaxial image planes and a 6-mm full-width-at-half-maximum resolution for a line source in the center field of view. The study was performed in a single bed position, with the dynamic data collected over the lower chest area to include the heart and the upper portion of the liver.

After positioning the participant in the PET scanner, a 15-min ^{68}Ga transmission scan was performed. Immediately afterward, the tracer dose of FDG, 200 ± 22 MBq (5.4 ± 0.6 mCi) was given intravenously slowly over 2 min. PET imaging and blood sampling began immediately when the injection was begun. PET images were obtained for 20 s each during the first 5 min, then for 1 min each during the following 10 min and then for 5 min each for the next 75 min. A blood sample was obtained as close as practical to the midpoint of each PET image. The actual time of blood collection was recorded and was used in the model analysis. At 90 min after the injection, the imaging and blood sampling were discontinued and a urine sample (representing cumulative bladder uptake of the FDG) was collected.

Sample Processing

Blood was collected in heparinized tubes. Samples (0.5 mL) of whole blood and of plasma from each blood sample were pipetted into well counter tubes, as were quadruplicate 0.5-mL samples of urine. ^{18}F activity in these samples was measured in a gamma well counter in comparison with a known aliquot of the injected dose. Activity was expressed as microcuries per milliliter and percentage dose per milliliter. Urine activity was multiplied by the sample volume to obtain cumulative excretion in percentage dose per milliliter.

Erythrocyte FDG concentration was estimated from the formula:

$$C_e = [C_{wb} - C_p \times (1 - \text{hct})]/\text{hct},$$

where C_e is erythrocyte FDG concentration, C_{wb} is whole-blood concentration and C_p is plasma concentration.

Whole-blood volume was estimated from an average of estimates using algorithms from the literature (*4,5*). Plasma and erythrocyte volumes were established assuming a whole-body hematocrit 0.9 times that of the peripheral blood. Plasma, erythrocyte and whole-blood concentrations were multiplied by their respective volumes to obtain the total percentage dose in the plasma, erythrocyte or whole-blood compartment.

PET Image Processing

The PET images were corrected for tissue attenuation and radioactive decay. They were standardized by use of normalization and blank scans to express the FDG content in microcurie per milliliter. The images were reviewed in each of the 47 transaxial slices obtained. Regions of interest (ROIs) for the myocardium, left ventricle (LV), right ventricle (RV), lung and liver were identified on a summed series of images from the last ten 5-min frames of the kinetic study. In six of the studies, low counting rates in the lung ROIs led to noisy data from a single plane, so multiple adjacent planes (ones that showed the lung clear of other activity) were summed for the last 50 min of the study also. The lung ROI was then drawn on that summed image.

Time-activity curves (in microcuries per milliliter) were then generated in the plane that best showed the respective organ. When multiple planes were summed for the lung ROI, the lung time-activity curves were generated from the summed planes and then were corrected for the number of planes. Organ activities from ROIs were then multiplied by the organ volumes assumed in the MIRD adult human phantom (*6*) and expressed as percentage dose per organ.

Mathematical Modeling

The data for total organ content of FDG for plasma volume, erythrocyte volume, myocardium, lungs and liver, as well as for total renal excretion, were entered into a SAAM30 (*7,8*) compartmental model (Fig. 1), referred to below as the kinetic FDG model. In addition to fitting the observed data, published parameters for FDG brain kinetics (*3*) were assumed and were incorporated into this model.

Additional modeling studies, also using SAAM30, compared whole-blood kinetics of FDG with LV, RV and lung FDG kinetics in a search for an optimal noninvasive surrogate for arterial cannulation. These are referred to below as the whole-blood models.

Modeling Strategy

FDG Kinetic Model. Initially, the kinetic model was set up with each of the measured organs represented by a single compartment in exchange with the plasma, plus (in the case of the myocardium, lungs and liver) an adjustable fraction of the plasma and erythrocyte compartments.

These blood organ compartment fractions represent blood physically contained in the organ measured and also any tissue compartment within that organ that exchanges with the plasma too rapidly to be separated out in the model fit. In addition to the measured organs, the brain was represented in the model by published parameters for gray matter and white matter (*3*). Unmeasured organs and tissues were represented by "fast exchange" and "slow exchange" compartments in a mammillary configuration with the plasma.

Because the tracer was given over a 2-min period, the dose was incorporated into the model as a 2-min infusion. The rate of appearance of the FDG into the central circulation was adjusted to fit the early data.

In fitting the liver data, it became apparent that the simple configuration (one compartment plus blood pool) initially used was not adequate. A second tissue compartment was added, with improvement in the fit both visually and statistically and with improvement in the sum of squares of deviation of the data from the model projection.

In the course of fitting the individual cases, we observed that the return parameters from the myocardial, lung and slow liver compartments frequently adjusted to zero, making those compartments functionally "sinks" for the FDG that reaches them. Because this concept is reasonable, in view of the known essentially unidirectional uptake of FDG in its practical use as a metabolic marker, we repeated the fits, setting those returns to zero in all cases. We found that the fits did not deteriorate visually. In addition, with this simpler configuration, the model became computationally identifiable. By analogy, we set the "unmeasured tissues" part of the model to a catenary configuration, with the slower compartment also a sink. This did not lead to deterioration of the model fit, and, by eliminating a parameter, made the other parameters identifiable.

The final model on which our results are based is illustrated in Figure 1. In it, the brain compartments remain exchangeable, as presented by Huang et al. (*3*), but with very slow return from the slow exchange brain compartments. The erythrocyte compartment

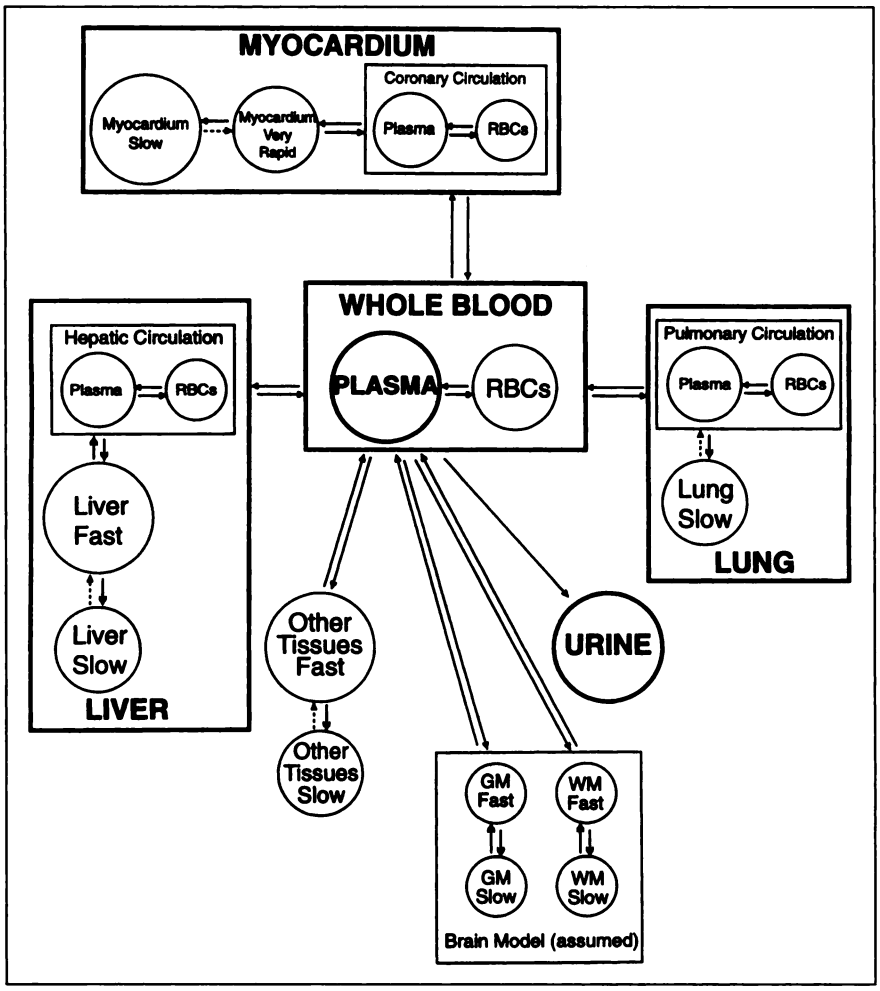

FIGURE 1. Model used to fit kinetic data. Units outlined in bold and labeled in uppercase letters represent observed data units. Dotted arrows are parameters set to zero in final fits of model to data. RBCs = red blood cells; GM = gray matter; WM = white matter.

is in rapid exchange with the plasma. The myocardium, liver and unmeasured tissues are each represented by an exchange compartment in series with a sink; although in the case of the myocardium, the kinetics of the exchange compartment are too rapid to resolve. It is possible that the lungs also have a very rapid exchange compartment, but any such compartment cannot be separated out from the lung blood content. Hence, the lungs are represented as a single compartment sink.

Whole-Blood Models. Models to assess the usefulness of PET quantification as a surrogate for arterial sampling of blood were set up comparing the whole-blood activity (in microcuries per milliliter) with the microcuries per milliliter in the ROI of the PET image.

Activity in the LV, RV and right lung was used for these comparisons. In these studies, the whole-blood activity was empirically fitted to a three-compartment mammillary model. Those parameters were then fixed, and the LV or RV lung data were fitted by adding an additional sink compartment as necessary. In addition, search was made for a simple algorithm to correct for the deviations between the paired datasets.

RESULTS

Fits of the Model to the Data

Figures 2 and 3 present the data and their fit to the model in one of the studies. Deviations in the fit such as that seen in the lung curve in Figure 3 were observed, but they were not consistent enough to justify adding further complexity to the model.

Parameters of Model Fit

The means and SDs and geometric means for the parameters for the final model fit are presented in Table 1. Each of these parameters represents the fraction of the donor compartment transferred to the recipient compartment each minute. Paired *t* tests demonstrated no significant differences between the parameters for the studies done in the fasting state and those associated with glucose administration. This is true even for the parameter for transfer into the myocardium. For this reason, the data for the 10 studies were combined. Table 2 presents summary parameter statistics for these combined data.

Tau Values

Table 3 contains the means, SDs and geometric means for the organ tau values calculated from the model fits of these 10 studies. As was true for the model fit parameters, paired *t* tests showed no statistically significant differences between tau values for the fasting and the glucose-fed states.

We compared the tau for the bladder in a variety of models for voiding time. Voiding at 120-min intervals was used to

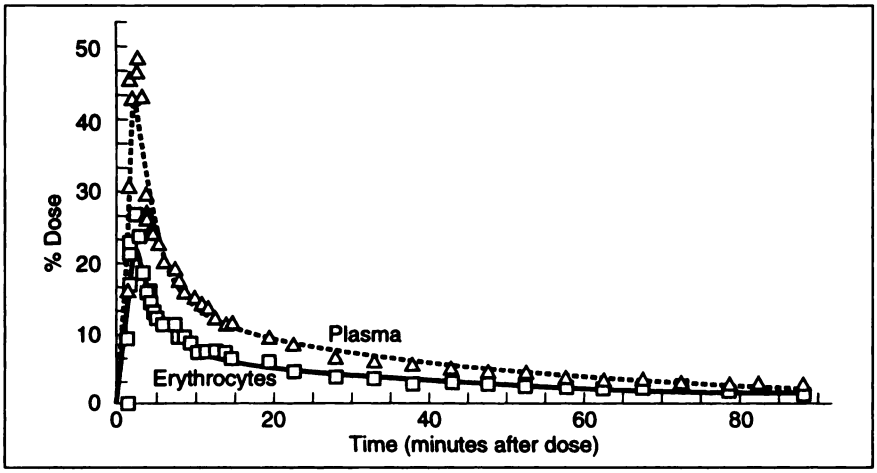

FIGURE 2. Subject G in first study: plasma and erythrocyte data compared with model projections.

compare our results with the results of Mejia et al. (*1*) and Jones et al. (*2*). We also examined 144- and 288-min intervals, because they correspond to the values used in several MIRD Dose Estimate Reports. We studied the impact on bladder tau of the voiding patterns of the patients receiving PET studies in our clinic, who generally void at 30 and 60 min after FDG. As shown in Table 3, tau is greatly reduced with more frequent voiding, especially early after dose administration. When a voiding pattern of 30, 60 and 120 min and every 120 min thereafter is compared with voiding every 120 min, the tau is only 41.1% ± 5.4% as great.

Projections from the Model

The geometric mean parameter values from Table 2 were used to build a "typical" model to project the overall decay-corrected distribution of FDG. Figure 4 shows projections from this model for distribution of FDG over the first 4 h after tracer administration. Of special interest is the large fraction of the activity in the unmeasured tissues and organs. This would include the skeletal muscles and gastrointestinal (GI) tract, which are known to concentrate FDG. These unmeasured compartments account for 76% of the decay-corrected FDG activity at infinity. On the other hand, the brain and the heart, which generally show the greatest FDG concentration, play a relatively small role in overall FDG economy because of their relatively small masses.

Plasma–Erythrocyte Exchange

Equilibrium of FDG between plasma and erythrocytes, as measured by the model, occurred very rapidly; mean residence time in the erythrocytes was 0.74 min. Pilot in vitro studies, in which blood was labeled with FDG and centrifuged after various time periods, both at room temperature and at 37°C, confirmed that equilibration of FDG between plasma and erythrocytes is very rapid.

Comparisons of Whole-Blood Activity with that in Left Ventricle and Right Ventricle PET Data

In general, early after the dose, there was good agreement between the data for microcuries per milliliter in the whole blood and the data generated by the ROIs of the LV and RV. However, the LV and RV data were rather noisy, because of the small volume represented in the ROI. In all cases, there was a gradual relative increase in the LV or RV curve compared with the whole blood. An example, from the data of the same study shown in Figures 2 and 3, is presented in Figure 5. To fit the LV data, it was necessary to assume that a

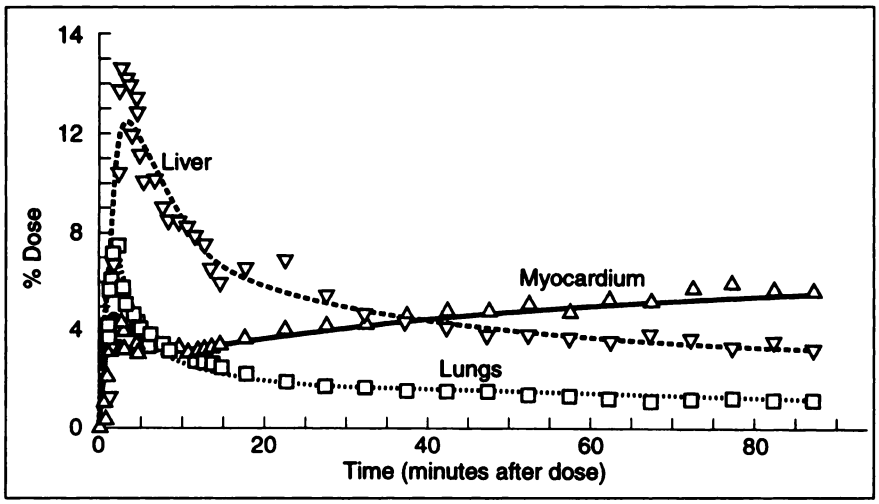

FIGURE 3. Subject G in first study: liver, myocardium and lung data compared with model projections.

TABLE 1
Parameters of Model Fit Comparing Glucose and Fasting Sessions

Parameter	Glucose sessions (n = 5)			Fasting sessions (n = 5)		
	Mean	SD	Geometric mean	Mean	SD	Geometric mean
Whole-body parameters						
Plasma to erythrocytes	5.31	2.75	4.79	4.30	3.31	3.46
Erythrocytes to plasma	9.17	1.86	8.98	6.98	3.44	6.02
Plasma to fast "other"	0.377	0.088	0.369	0.365	0.169	0.328
Fast "other" to plasma	0.109	0.048	0.100	0.095	0.015	0.094
Fast "other" to slow "other"	0.0180	0.0091	0.0155	0.0154	0.0057	0.0146
Plasma to urine	0.0085	0.0024	0.0081	0.0091	0.0022	0.0088
Myocardial parameters						
Plasma to myocardium	0.0055	0.0031	0.0037	0.0051	0.0058	0.0024
Fraction of blood volume "seen"*	0.066	0.013	0.065	0.073	0.008	0.072
Lung parameters						
Plasma to lung	0.0017	0.0007	0.0016	0.0017	0.0006	0.0016
Fraction of blood volume in lung	0.149	0.034	0.146	0.150	0.043	0.146
Liver parameters						
Plasma to liver exchange	0.0771	0.0583	0.0552	0.0584	0.0838	0.0262
Liver exchange to plasma	0.219	0.108	0.186	0.162	0.145	0.120
Liver exchange to liver "sink"	0.0120	0.0073	0.0095	0.0233	0.0327	0.0032
Fraction of blood volume in liver	0.192	0.096	0.174	0.294	0.225	0.235

*About 2% of blood volume is estimated for coronary artery content. Balance represents the "very rapid" myocardial exchange pool. Table shows fraction of donor compartment transferred to recipient compartment each minute.

fraction of the myocardium, in this case 11.2%, was "seen" by the LV. This fraction proved to be extremely variable, and it became apparent that a normalization of the curve would be necessary.

TABLE 2
Parameters of Model Fit, Combined Data (n = 10)

Parameter	Combined data from glucose and fasting sessions		
	Mean	SD	Geometric mean
Whole-body parameters			
Plasma to erythrocytes	4.80	2.92	4.07
Erythrocytes to plasma	8.07	2.85	7.35
Plasma to fast "other"	0.371	0.127	0.348
Fast "other" to plasma	0.102	0.034	0.097
Fast "other" to slow "other"	0.0167	0.0073	0.0150
Plasma to urine	0.0088	0.0022	0.0085
Myocardial parameters			
Plasma to myocardium	0.0053	0.0044	0.0030
Fraction of blood volume "seen"*	0.069	0.011	0.068
Lung parameters			
Plasma to lung	0.0017	0.0006	0.0016
Fraction of blood volume in lung	0.150	0.036	0.146
Liver parameters			
Plasma to fast liver compartment	0.068	0.069	0.038
Fast liver compartment to plasma	0.219	0.108	0.186
Fast liver to liver "sink"	0.018	0.023	0.006
Fraction of blood volume in liver	0.243	0.172	0.202

*About 2% of blood volume is estimated for coronary artery content. Balance represents the "very rapid" myocardial exchange pool.

Table shows fraction of donor compartment transferred to recipient compartment each minute.

Comparisons of Whole-Blood Activity with that in PET Lung Data

Use of the lung data, especially that from the right lung, has the potential advantages that a large volume can be measured, so as to reduce the "noise" in the data, and that there is little or no interference from the myocardium. It has

TABLE 3
Summary of Tau Values Calculated from 10 Studies

Compartment	Mean	SD	Geometric mean
Plasma volume	0.171	0.060	0.161
Red blood cell volume	0.095	0.032	0.089
Heart	0.133	0.065	0.115
Lungs	0.084	0.028	0.079
Liver	0.161	0.057	0.150
Whole brain	0.245	0.090	0.230
Gray matter	0.174	0.064	0.164
White matter	0.070	0.026	0.066
Bladder, no void	0.227	0.087	0.216
Bladder, clinical*	0.040	0.017	0.039
Bladder, void at 120 min	0.101	0.041	0.095
Bladder, void at 144 min	0.119	0.047	0.113
Bladder, void at 288 min	0.191	0.075	0.181
Whole body 1†	2.639	NA	2.639
Whole body 2‡	2.412	0.087	2.410
Whole body 3§	1.790	0.139	1.785

*Bladder, clinical: voiding at 30, 60 and 120 min, then every 120 min.

†Assuming no excretion and including all organs and tissues.

‡Taking urinary excretion into account, but including all organs and tissues.

§Excluding urine, heart, brain, lung and liver.

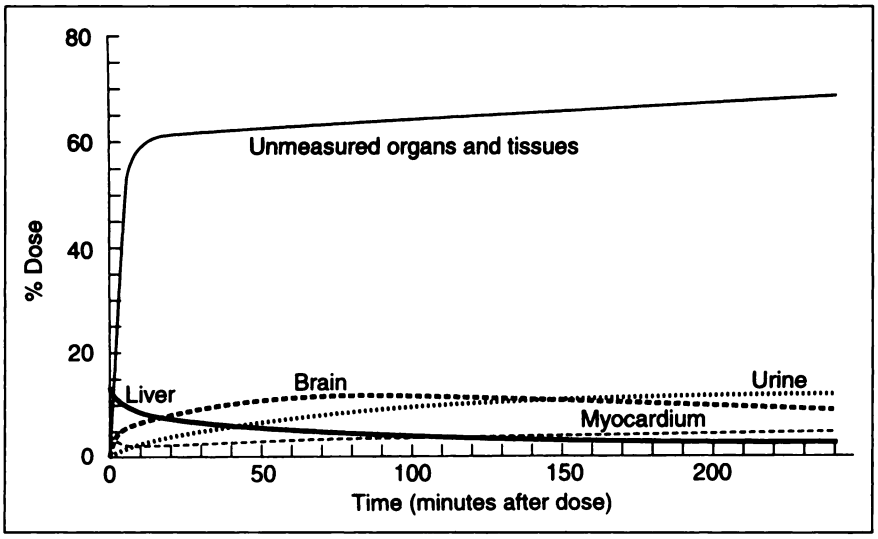

FIGURE 4. Projections of model using geometric means of parameters derived from 10 studies (*3*). Unmeasured organs and tissues curve is sum of fast and slow other tissues compartments illustrated in Figure 1.

the disadvantage that one must correct both for the fraction of the lung ROI represented by blood and for uptake by the lung itself. Figure 6 shows the whole-blood and right lung data from the same study, with the lung data corrected for the blood fraction seen in the lung by the model. It was also necessary to correct for a lung uptake of 0.63% ± 0.17% of whole-blood activity per minute to fit the right lung data.

The lung data have little statistical noise, so they are desirable as a source of projected blood activity. If it were possible to use the population mean lung uptake of FDG to predict the shape of the whole-blood activity from the right lung activity, it would then be possible to superimpose the two curves by comparing a single late venous blood sample with the simultaneous lung observation. However, our solution using this population mean led to unacceptable deviations from the observed data in some cases.

We then explored the feasibility of using a series of peripheral venous blood-to-right lung ratios to project the whole-blood data, using a simple linear or logarithmic fit of the ratio. For this study, we used blood samples taken at 5 and 10 min and then every 10 min, plotting the ratio of their activity (as microcuries per milliliter) to the activity (as microcuries per milliliter) in simultaneous lung images. We started at 5 min, because, by that time the venous and arterial FDG have almost reached equilibrium (*9*). We did both linear and logarithmic fits of the ratios and then used them to generate the whole-blood curve. The sum of squares for fit of this projection to the observed whole-blood data was 5% better with a linear fit than with a logarithmic fit.

The observed and calculated whole-blood data for the same illustrative case, calculated from a linear fit of the whole-blood-to-right lung ratios, are presented in Figure 7. The upper section of Figure 7 shows the first 5-min fit, demonstrating the relative lag of peripheral arterial blood compared with the pulmonary circulation. The entire curve is shown in the lower portion. Similar good projections from right lung to whole-blood data were obtained in all 10 studies.

DISCUSSION

The model presented in this article is a synthesis of the available submodels available for projections of FDG activity after intravenous administration to humans. It is compatible with the published data on the distribution and radiation

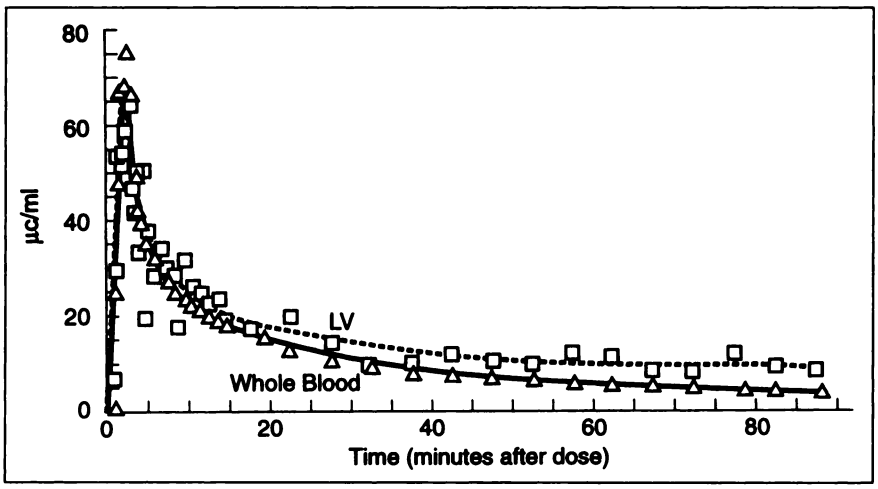

FIGURE 5. Comparison of data from same subject in Figures 1, 2 and 3: μCi/mL in peripheral whole blood and in LV.

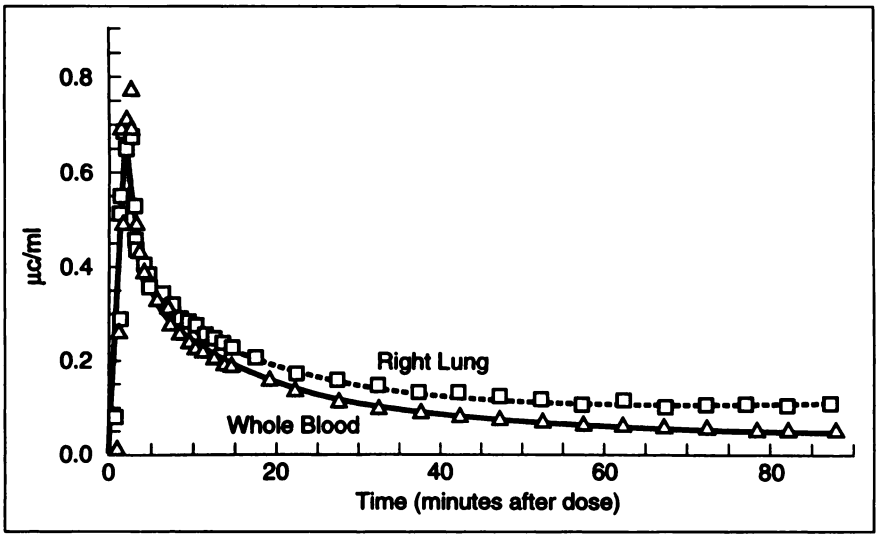

FIGURE 6. Same as Figure 5, but right lung data are compared instead of LV, divided by blood fraction from model.

dosimetry of FDG. As new submodels are developed for FDG kinetics in other organs or tissues of interest, these can be incorporated into this overall model.

The tau values calculated from this model for the heart, liver, lung and bladder (120 min void) can be compared with those published by Mejia et al. (*1*) and Jones et al. (*2*). Our mean tau value for the heart is 0.133 ± 0.063, compared with 0.085 ± 0.020 of Mejia et al. In the case of the liver, our

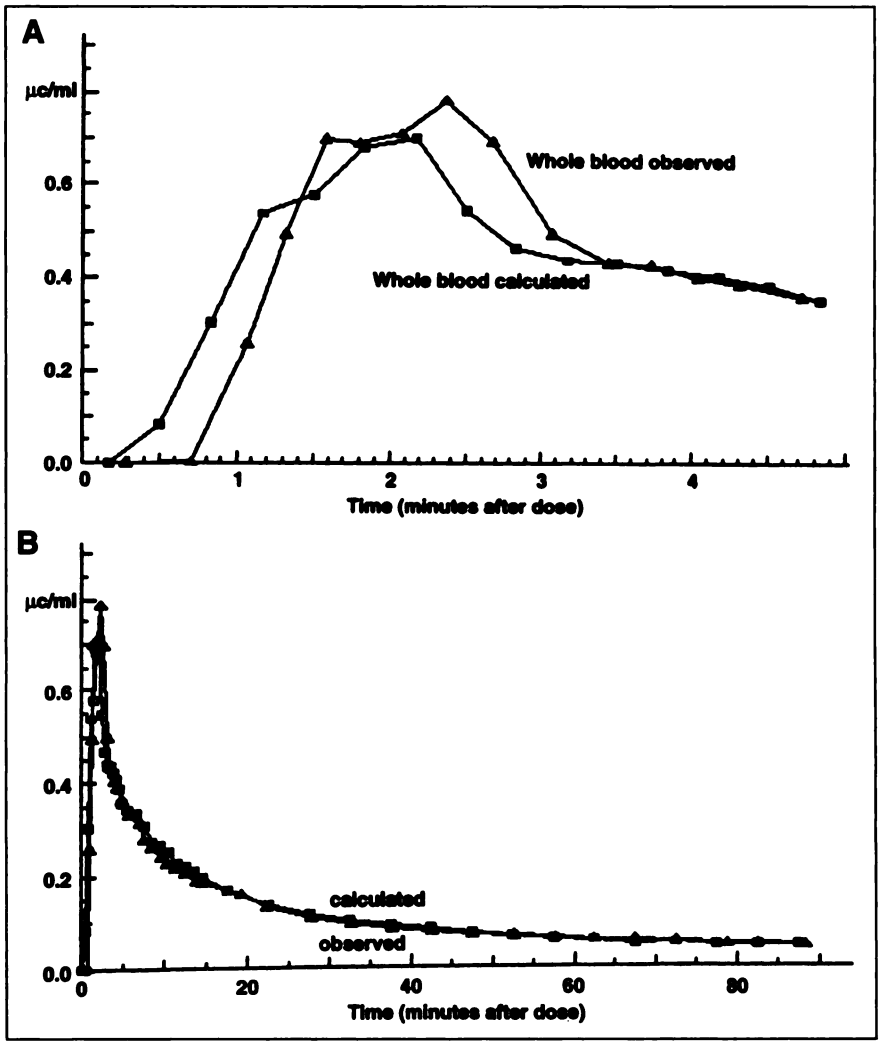

FIGURE 7. Observed whole-blood data in same study, compared with that calculated from right lung data corrected by linear fit of late blood-to-lung ratios. (A) First 5-min blood data observed and calculated. This shows earlier appearance of tracer in lung than in peripheral artery. (B) Observed and calculated blood data for entire 90-min study.

mean tau is 0.161 ± 0.057, whereas that of Mejia et al. is 0.112 ± 0.030. For the lungs, we found tau to be 0.074 ± 0.032, whereas the value of Mejia et al. was 0.023± 0.003. In the case of the bladder, assuming voiding every 120 min, our average tau is 0.101 ± 0.041, compared with 0.123 ± 0.046 of Mejia et al. and 0.198 ± 0.109 of Jones et al. There were methodological differences among the studies, as well as biologic variability. In no case was the difference among these studies statistically significant. When our three studies with incomplete blood data are added to the series reported here, the mean taus become 0.128 for heart, 0.149 for liver, 0.074 for lungs and 0.091 for the bladder with voiding every 120 min.

We found that tau for the bladder was sensitive to early emptying of the bladder, with a 59% reduction in radiation dose when the participant voids at 30, 60 and 120 min and every 120 min thereafter, compared with voiding every 120 min. We should point out, however, that our model does not allow for the varying dosimetry of the bladder contents as the bladder size changes. Studies of bladder dosimetry of FDG by Dowd et al. (*10*) and by Thomas et al. (*11*), expanding on a variable-sized bladder model developed by Chen et al. (*12*), demonstrate the effect of a large bladder volume in sparing the bladder wall. This effect, as well as the frequent voiding that our study emphasizes, can be achieved by forcing of fluids. We recommend that, when feasible, high fluid intake and early and frequent voiding after FDG administration be encouraged.

Our study of FDG equilibration between plasma and erythrocytes confirms the validity of using either plasma or whole-blood FDG measurements and converting from one to the other using the hematocrit. In kinetic studies, plasma is generally assumed to be the central compartment for organ distribution. On the other hand, it may be more convenient to measure whole blood, especially if PET images are used as proxy for arterial blood sampling.

We found that the LV, RV, left lung and right lung all had limitations as proxies for whole arterial blood sampling. In all of these cases, there was increasing activity in the PET images compared with whole-blood activity. In the case of the LV and RV, this is most likely due to some myocardial FDG in the ROI, despite our efforts to avoid the myocardium. Because our studies were not gated, myocardial contamination of the chamber image is to be expected. On the other hand, this digression between the curves occurred even when very little myocardial activity could be found in the images, a result that we are at a loss to explain.

The data curves for the lungs are smoother than those for the LV and RV, because it is possible to sample a large volume of lung. In 9 of the 10 studies, the left lung data were greater than those for the right lung, due to a minimal amount of myocardial activity despite our efforts to avoid the heart in drawing the lung ROIs. The right lung activity was free of myocardial influence. Nevertheless, the right lung curve also digressed from the arterial blood curve, due to FDG uptake in the lung tissue itself. Fortunately, it is possible to correct satisfactorily for this digression by a simple linear factor derived from a series of venous blood samples. Based on these studies, we believe that the best noninvasive proxy for arterial blood sampling is a series of venous blood samples obtained subsequent to the first 5 min after intravenous tracer administration, combined with a large volume PET ROI of the right lung, using a linear correction factor.

The large fraction of the dose remaining in the unsampled tissues and organs is consistent with the whole-body components found by Mejia et al. (*1*) and Jones et al. (*2*), who placed 74.4% and 70%, respectively, of total FDG activity in this category. This finding is compatible with the large amount of activity sometimes seen in FDG PET studies in the skeletal muscle and GI tract and with the fact that they are large organs. A study of whole-body FDG distribution in the mouse, in progress in our department, also shows that a large fraction of the dose is in the residual tissues (D. Goodwin, personal communication, 1997).

CONCLUSION

The model in this article fitted the variety of data collected in this study well. This model is sufficiently general that it can be expanded to include other aspects of FDG kinetics as the results of new studies become available.

Specific findings in the application of the model are the following:

1. Glucose loading state is a poor predictor of myocardial FDG uptake.
2. The majority of FDG distribution at 90 min is in tissues other than the blood, brain, heart and liver.
3. Bladder radiation will be much reduced if the patient forces fluids and voids early after FDG administration.
4. Summed activity of a large right lung volume, normalized to venous blood late in the study, is a good proxy for arterial blood sampling.

ACKNOWLEDGMENTS

We thank the staff of the Nuclear Medicine and Anesthesia Services for their patience and assistance in making this study possible. Carol Stepp and Irene Pereira provided skillful and essential technical support. Thanks also to Regitze Bongsgaard Schambye, MD, and Nan-Jing Peng, MD, who participated in some of the experimental sessions. A special thanks to our veteran patients who volunteered for these studies.

The FDG for this study was provided without charge by PET Net (Palo Alto, CA). The mathematical modeling was supported in part by the Medical Research Service of the Department of Veterans Affairs.

REFERENCES

1. Mejia AA, Nakamura T, Masatoshi I, Hatazawa J, Masaki M, Watanuki S. Estimation of absorbed doses in humans due to intravenous administration of fluorine-18-fluorodeoxyglucose in PET studies. *J Nucl Med.* 1991;32:699–706.

2. Jones SC, Alevi A, Christman D, Montanez I, Wolf A, Reivich M. The radiation dosimetry of 2-[F-18]fluoro-2-deoxy-D-glucose in man. *J Nucl Med.* 1983;23:613–617.
3. Huang S-C, Phelps ME, Hoffman EJ, Sideris K, Selin CJ, Kuhl DE. Noninvasive determination of local cerebral metabolic rate of glucose in man. *Am J Physiol: Endocrinol Metab.* 1980;238:69–82.
4. Belcher EH, Vetter H. *Radioisotopes in Medical Diagnosis.* New York, NY: Appleton-Century-Crofts; 1971:335.
5. Iturraide MP. *Dictionary and Handbook of Nuclear Medicine and Clinical Imaging.* Boca Raton, FL: CRC Press; 1990:460–461.
6. Snyder WS, Ford MR, Warner GG. *Estimates of Specific Absorbed Fractions for Photon Sources Uniformly Distributed in Various Organs of a Heterogeneous Phantom.* Medical Internal Radiation Dose Pamphlet No. 5, revised. New York, NY: Society of Nuclear Medicine; 1978.
7. Berman M, Beltz WF, Greif PC, Chabay R, Boston, RC. *Consam: User's Guide.* Washington, DC: Department of Health and Human Services; 1983.
8. Berman M, Shahn E, Weiss MR. The routine fitting of kinetic data to models: formulation for digital computers. *Biophys J.* 1962;2:275–287.
9. Phelps ME, Huang SC, Hoffman EJ, Selin C, Sokoloff L, Kuhl DE. Tomographic measurement of local cerebral glucose metabolic rate in man with 2-(F18)fluoro-2-deoxy-D-glucose. *Ann Neurol.* 1979;6:371–388.
10. Dowd MT, Chen C-T, Wendel MJ, Faulhaber PJ, Cooper MD. Radiation dose to the bladder wall from 2-^{18}F-fluoro-2-deoxy-D-glucose in adult humans. *J Nucl Med.* 1991;32:707–712.
11. Thomas SR, Stabib MG, Chen C-T, Samaratunga RC. MIRD Pamphlet No. 14. revised: a dynamic urinary bladder model for radiation dose calculations. *J Nucl Med.* 1999;40:102S–123S.
12. Chen C-T, Harper PV, Lathrop KA. A simple dynamic model for calculating radiation absorbed dose to the bladder wall. In: Schlafke-Stelson AT, Watson EE, eds. *Fourth International Radiopharmaceutical Dosimetry Symposium,* November 5–8, 1985. Oak Ridge, TN: U.S. Department of Energy; 1986:587–612.